Thermal Fragmentation of 3-Vinyloxetane: A Quantum Chemical Study

S. Calvo-Losada, F. Enríquez, J. Martín-Ortiz, and J. J. Quirante*

Departamento de Química Física, Facultad de Ciencias, Universidad de Málaga, Campus de Teatinos s/n, 29071 Málaga, Spain

Received: November 7, 2002

3-Vinyloxetane undergoes fast thermal fragmentation as compared with oxetane or alkyloxetanes. To explain this kinetic effect, a quantum chemical investigation of the thermal decomposition of 3-vinyloxetane was carried out by the B3LYP density functional method and by the MP2 and QCISD ab initio theories using the 6-31G(d) basis set. Relative energies were evaluated on the basis of single-point QCISD(T)/cc-pVDZ energies. Computational results were properly interpreted by means of configurational analysis of wave functions and by analyzing the electronic charge density $\rho(r)$ and related fields within the framework of the atoms in molecules theory. Our results predicted both the synchronous and the asynchronous concerted paths for the direct fragmentation to products. However, for the asynchronous one no biradical minimum was obtained. A two-step pathway that implies a ring expansion to 3,6-dihydro-2*H*-pyran was also studied. The asynchronous concerted path, assisted by an unexpected H-interaction, resulted in the most favorable reaction channel and would explain the increase of fragmentation rate of oxetanes upon symmetric substitution by a vinylic group.

Introduction

Oxetane chemistry is becoming increasingly important because the oxetane ring is present in relevant naturally occurring compounds (taxol, oxetanocin, thromboxane A, etc.), in some cases being crucial for maintaining the activity, for example, in taxol. Particularly, the pyrolysis of oxetane is important because oxetanes are intermediates in the oxidation of hydrocarbons.

There are some interesting similarities in the thermal decomposition of oxetane and cyclobutane that extend to their simple alkyl and vinyl derivatives.[1] For instance, a vinyl substitution in either oxetane (at the C3 position) or cyclobutane increases dramatically their fragmentation reaction rates by a factor greater than 200 with respect to reaction rates for the unsubstituted compounds. To explain this kinetic effect in the two types of substances, a ring expansion has been suggested as an alternative reaction channel (see Scheme 1). However, the performance of this hypothesis is not clear for oxetanes. Carless et al. have shown,[1a] from a careful kinetic study of thermal fragmentation of *cis*-2,4-dimethyl-*trans*-3-vinyloxetane (CDVO), that the six-center intermediate of the ring expansion pathway, *cis*-2,6-dimethyl-3,6-dihydro-2*H*-pyran (CDHP), decomposes 6−7 times faster than CDVO. These authors have reported that the ring expansion path contributes only 2−3% to the overall reaction, estimating that the direct fragmentation of CDVO should be 40 times faster than the path via CDHP.

To date, there has been little published work on the pyrolysis of oxetanes (which contrasts sharply with the great amount of data reported on cyclobutanes). Concerning its mechanism, to our knowledge, only the theoretical work by Robb and co-workers on the formation of oxetane by photochemical addition of carbonyl compounds to alkenes (the Paterno−Buchi reaction) has dealt with formation or decomposition of oxetanes.[2] These authors reported a MC-SCF/6-31G(d) study of the singlet and triplet Paterno−Buchi photochemical reaction (ethylene plus formaldehyde to originate oxetane), in which they characterize the relevant minima and transition structures on the S_0, S_1, and T_1 potential energy surfaces (PES) and even two S_0/S_1conical

SCHEME 1: Direct Fragmentation (Route I) and Ring Expansion Processes (Route II)

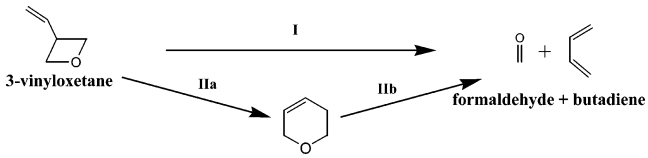

intersections in the Born−Oppenheimer violation regions, where a fast decay from the S_1 to the S_0 ground state takes place. For the S_0 electronic state Robb et al. characterized biradical channels for both the C---O and the C---C possible attacks. For each, gauche and trans biradical intermediates were obtained, the former being more important because trans pathways only represent an indirect route to the gauche region, where the final cyclization takes place. Two transition states relate the S_0 biradical intermediates with the oxetane or reactants minima over a small barrier (2.7 and 1.9 kcal/mol for the C---O attack and 0.2 and 1.2 kcal/mol for the C---C attack). Concerted paths in the S_0 state were not reported in this study.

Another study by Bordejé and co-workers reported the gas-phase basicity of oxetane and its O-protonation effects, which they determined experimentally and theoretically.[3]

In this work the thermal pyrolysis of C3-vinyl substituted oxetanes will be theoretically studied by means of density functional theory (DFT),[4] and the computational results will be interpreted by means of a configurational analysis of the wave function[5] and by analyzing the electronic charge density $\rho(r)$ and related fields within the framework of the atoms in molecules theory.[6] Thus, we will shed some light on the effects of the vinyl substituent on the energy barriers of the thermal decomposition of oxetanes.

Theoretical Methods

Calculations were carried out using the Gaussian94 and Gaussian98 suites of programs.[7] Density functional calculations

10.1021/jp022373n CCC: $25.00
Published on Web 04/01/2003

were performed with the B3LYP functional[8] and with the 6-31G(d) basis set.[9] Density functional theory seems to cover significant correlation effects in an unspecified manner[10a] and has proven useful in both the description of typical single-determinantal and also in some multireference problems where the wave function is still dominated by one configuration.[10b−d] For instance, DFT studies of a variety of pericyclic and other reactions by using gradient-corrected and hybrid functionals have been reported to render information within chemical accuracy as compared with experimental data.[10e−g] In particular, a recent paper on the thermal rearrangement of norcardiene reinforced the ability of DFT(B3LYP) versus multireference calculations in the treatment of sigmatropic rearrangements.[11] Furthermore, such DFT methods appear to treat both closed- and open-shell structures in a more balanced fashion, which is essential for the study of pericyclic reactions that may occur either concerted (via closed-shell species) or stepwise (via open-shell species).[10e]

The stable species were fully optimized and the transition states (TS) were located by means of the Schlegel algorithm at the B3LYP/6-31G(d) level.[12] All critical points were further characterized by computing the analytic frequencies at the same theoretical level. Reoptimizations at MP2/6-31G(d)[13] and analytic frequencies at the same level of theory are also reported when available to compare with the DFT results. For selected and dubious structures, optimizations at QCISD/6-31G(d)[14] and subsequent QCISD(T) single point calculations employing the cc-pVDZ Dunning's correlated basis set[15] (i.e., QCISD(T)/cc-pVDZ//QCISD/6-31G(d) calculations) were also done. QCISD is a correlated size-consistent method derived (like the MP*n* methods) from the HF single reference wave function, but in this case by means of a CI expansion of singles and doubles excitations. In the QCISD(T), triple electronic correlation effects are also estimated, in a perturbative manner.[14]

The biradical region of the PES was investigated at the UB3LYP/6-31G(d) level of theory. Cremer et al.[10d] have shown that unrestricted DFT (UDFT) calculations with the semiempirical B3LYP functional is also capable of compensating for some static electron correlation and should provide reasonable results in the case of some typical organic biradicals. UDFT results have been reported to be comparable and even superior to those obtained with CASSCF methods for a variety of pericyclic reactions. However, the usefulness of the UDFT approach must be analyzed from case to case.[16]

The influence of truncation effects of the basis set on the relative energies was estimated by single-point energy calculations with the 6-311+G(d,p) basis set on the B3LYP/6-31G(d) optimized geometries.[9] Reaction paths on the potential energy surfaces passing through the TSs studied in this work were followed by the B3LYP/6-31G(d) intrinsic reaction coordinate (IRC)[17] calculations using the González and Schlegel algorithm.[18]

To obtain a more chemically graspable picture of the reactive processes, the TSs for the [2+2] and [2+4] cycloreversion processes were analyzed by means of a theoretical method originally developed by Fukui.[19] This interpretative tool rewrites a TS monodeterminantal wave function (built in this work from the UB3LYP/6-31G(d,p) MOs) as a combination of the electronic configurations of the interacting fragments,

$$\Psi = c_o\Psi_o + \sum_q c_q\Psi_q \qquad (1)$$

where Ψ_o is the reference-state function in which neither electron transfer nor electron excitation takes place and Ψ_q stands for monotransferred configurations (an electron of an occupied MO in any fragment is transferred to an unoccupied MO of a different one), monoexcited configurations (where the electron is excited to an unoccupied MO of the same fragment), ditransferred, and so on. These contributions were estimated with the ANACAL program developed by López et al.,[5b] which has proven usefulness for understanding the chemical features of complex formation and chemical reactivity.[5]

Finally, for a better understanding of electronic rearrangements along the studied processes, we analyzed the topology of the electronic charge density, $\rho(r)$, at different stages of the reaction paths, by using the atoms in molecules theory of Bader.[6] In this scheme the critical points of $\rho(r)$, i.e., (3,−3), (3,−1), (3,+1), and (3,+3), characterize the nuclei, bonds, rings, and cages in the molecule respectively, and fulfill the Poincaré−Hopf relationship (nuclei − bonds + rings − cages = 1). The associated gradient vector field, $\nabla\rho(r)$ serves to further confirm the existence of atomic interactions, because, according to Bader, the presence of a bond path linking two nuclei, as defined by a trajectory of $\nabla\rho(r)$, provides the necessary and sufficient conditions for two atoms be bonded one another.[6] The Laplacian distribution of $\rho(r)$, $\nabla^2\rho(r)$, is of primary importance in chemical reactivity given that it determines the loci of preferential accumulation and depletion of charge density and therefore the regions of electrophillic or nucleophillic attack, respectively. The analysis of the properties of $\rho(r)$ evaluated at the BCPs [ρ_c, $\nabla^2\rho_c$ and the eigenvalues of the Hessian matrix of $\rho(r)$, λ_1, λ_2, and λ_3 (note that $\nabla^2\rho(r)$ equals $\lambda_1 + \lambda_2 + \lambda_3$), and the ellipticity, ϵ] enables one to characterize the atomic interactions. Covalent or shared interactions have large values of both $\rho(r)$ and $\nabla\ ^2\rho(r)$, the latter being negative. On the contrary, the closed-shell interactions (ionic, van der Waals, and the like) exhibit low values of both quantities, $\nabla^2\rho(r)$ being positive, indicating that the charge density is preferentially accumulated in the shells of the atoms. This is also seen in the values of λ_1 and λ_2, which indicate preferential accumulation of charge density in perpendicular planes to the bond path, and the λ_3 eigenvalue, which indicates contraction of charge along the bond path toward the nuclei. Different values of λ_1 and λ_2 involve an elliptical distribution of $\rho(r)$ around the bond path thereby the name of "ellipticity" for the relation $\lambda_1/\lambda_2 - 1$. The charge densities were derived at the B3LYPY/6-31G(d)//B3LYP/6-31G(d) and B3LYP/6-311+G(d,p)//B3LYP/6-31G(d) levels. The former density presents some spurious critical points (for example for TS6, see below) that disappear at the higher theoretical level. The analysis of the topology of the charge density, $\rho(r)$, was carried out with the EXT94b subroutine of the AIMPAC[20a] suite of programs and the automated MORPHY1.0 and MORPHY98 programs developed by P. L. A. Popelier.[20b,c]All the magnitudes are in a.u. unless otherwise noted.

Results and Discussion

Relevant structural data for the located stationary points (minima and TSs) of the B3LYP/6-31G(d) PES are summarized in Figures 1 and 2. For comparisons, MP2/6-31G(d) and QCISD/6-31G(d) results are also included when convergence was achieved.

For the structures reported in this work, the UB3LYP/6-31G(d) wave functions did not show spin contamination at all ($\langle S^2\rangle = 0$) and both the RB3LYP and UB3LYP formulations rendered the same results. UDFT produces a set of α and β orbitals in analogy with the unrestricted HF method, and several authors had pointed out that the Kohn−Sham determinantal wave

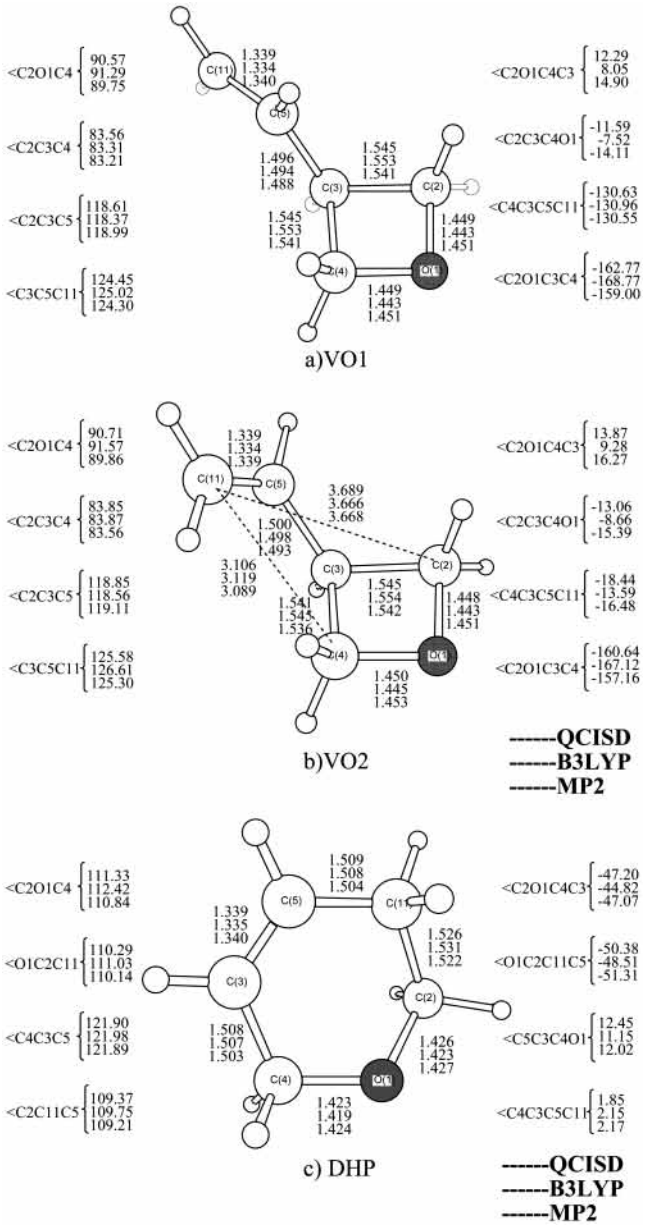

Figure 1. Optimized structures for anti (VO1) and gauche (VO2) conformers of 3-vinyloxetane and for the 3,6-dihydro-2*H*-pyran intermediate (DHP). Other rotamers such as the syn one (VO3) or the second gauche one (VO4), equivalent to VO2, were omitted for simplicity.

function should exhibit some spin contamination for open-shell systems. However, in density functional methods the emphasis falls on the electronic density, which appears to be less sensitive to spin contamination than the wave function. In consequence, UDFT results, in contrast to UHF, have lower spin contamination effects.[10a]

Owing to substitution symmetry, 3-vinyloxetane can undergo two equivalent fragmentation modes, but only those implying C3−C2 and/or C4−O1 oxetane bonds were considered. Table 1 compiles relative energies referred to the global minimum-energy geometry of 3-vinyloxetane, computed at B3LYP/6-31G(d)//B3LYP/6-31G(d) and B3LYP/6-311+G(d,p)//B3LYP/6-31G(d) levels. MP*n* and QCISD(T) energies are also included in Table 1.

Scheme 2 displays the possible routes from 3-vinyloxetane to give products (formaldehyde plus *cis*- or *trans*-butadiene). For the direct formation of the products (reaction I in Scheme 1, and Scheme 2) several reaction channels were obtained, differing from one another by the asynchronicity and the relative orientation of the emerging fragments. For reaction IIa in Scheme 1 (formally an intramolecular [1,3]-sigmatropic shift) two reaction paths were characterized to render the 3,6-dihydro-2*H*-pyran (DHP) that corresponds to the allowed-stereochemical courses for this pericyclic atomic migration. Finally, a concerted fragmentation of DHP toward products was found (step IIb in Scheme 1, and Scheme 2). The more relevant features of these paths will be separately presented in the following three sections. The last two sections will be devoted to the configurational analysis of the TS's wave functions and the AIM analysis of the charge density, respectively.

(a) Highly Synchronous Paths. The TS1 and TS2 transition states in Figure 2 (see also Scheme 2) correspond to the synchronous cleavage of the 3-vinyloxetane. TS1 connects the anti form of the reactant (VO1 in Figure 1) with the trans butadiene + formaldehyde product channel whereas TS2 connects a gauche rotamer of the reactant (VO2 in Figure 1) with the cis reaction products. On the basis of their structural features, TS1 and TS2 represent a highly concerted mechanism for the [2+2] cycloreversion process in which the two bonds are breaking simultaneously. According to the microscopic reversibility principle, TS1 and TS2 also correspond to a concerted mechanism for the thermal [2+2] cycloaddition reverse process, with quasi-parallel approximation of the molecular planes, which allows a more favorable orbital interactions between the fragments (see section d below).

Activation energy barriers of ca. 56 kcal/mol were obtained for both the TS1 and TS2 concerted fragmentation pathways. The overall process is predicted to be slightly exothermic, with a ΔE of −6.5 kcal/mol. This value is quite similar to that reported for the formaldehyde + ethylene parent reaction at CASSCF/6-31G(d) (−7.7 kcal/mol).[2]

The thermal "head-to-tail" dimerization of fomaldehyde shows some similarities with the reaction studied in this work. In a wide and excellent study on polar [2+2] cycloaddition (at the MC−SCF/4-31G level), Bernardi et al.[21] concluded that polar effects seem to modify the concerted region of the PES and to introduce the possibility of a concerted path competing with the biradical pathway. Bernardi et al. reported a transition structure that was very similar to both the TS1 and the TS2 discussed above. However, Bernardi's concerted TS had a C_{2h} distorted rectangular geometry and exhibits a small second imaginary frequency corresponding to the rotation of the two interacting fragments around the midpoints of their two CO bonds. The concerted path via this transition structure was about 2 kcal/mol higher in energy than the biradical one (computed at the MC−SCF/6-31G(d)//MC−SCF/4-31G level).

(b) Asynchronous Paths. Recent DFT results on the prototypical Diels−Alder and other pericyclic reactions encouraged us to systematically explore the nonsynchronous region of the PES with DFT methods.[10e,f] In principle, two modes of attack are possible (i.e., C---C and C---O attacks). Nevertheless, no evidence of asynchronous C---C paths was found on the PES. On the contrary, two very asynchronous transition structures (see Scheme 2 and TS3 and TS4 in Figure 2c,d) were located for the C---O attack at the restricted and unrestricted B3LYP/6-31G(d) levels. Because either B3LYP/6-31G(d) or UB3LYP/6-31G(d) calculations did not yield any biradical intermediates, TS3 (554.6i cm^{-1}) and TS4 (186.5i cm^{-1}) seemed "a priori" transition states for the direct formation of the products.

As shown in Table 1, TS3 lies 0.7 kcal/mol in energy below TS4 and about 2 kcal/mol below the highly synchronous TS1 or TS2. A subsequent IRC calculation confirmed that TS3

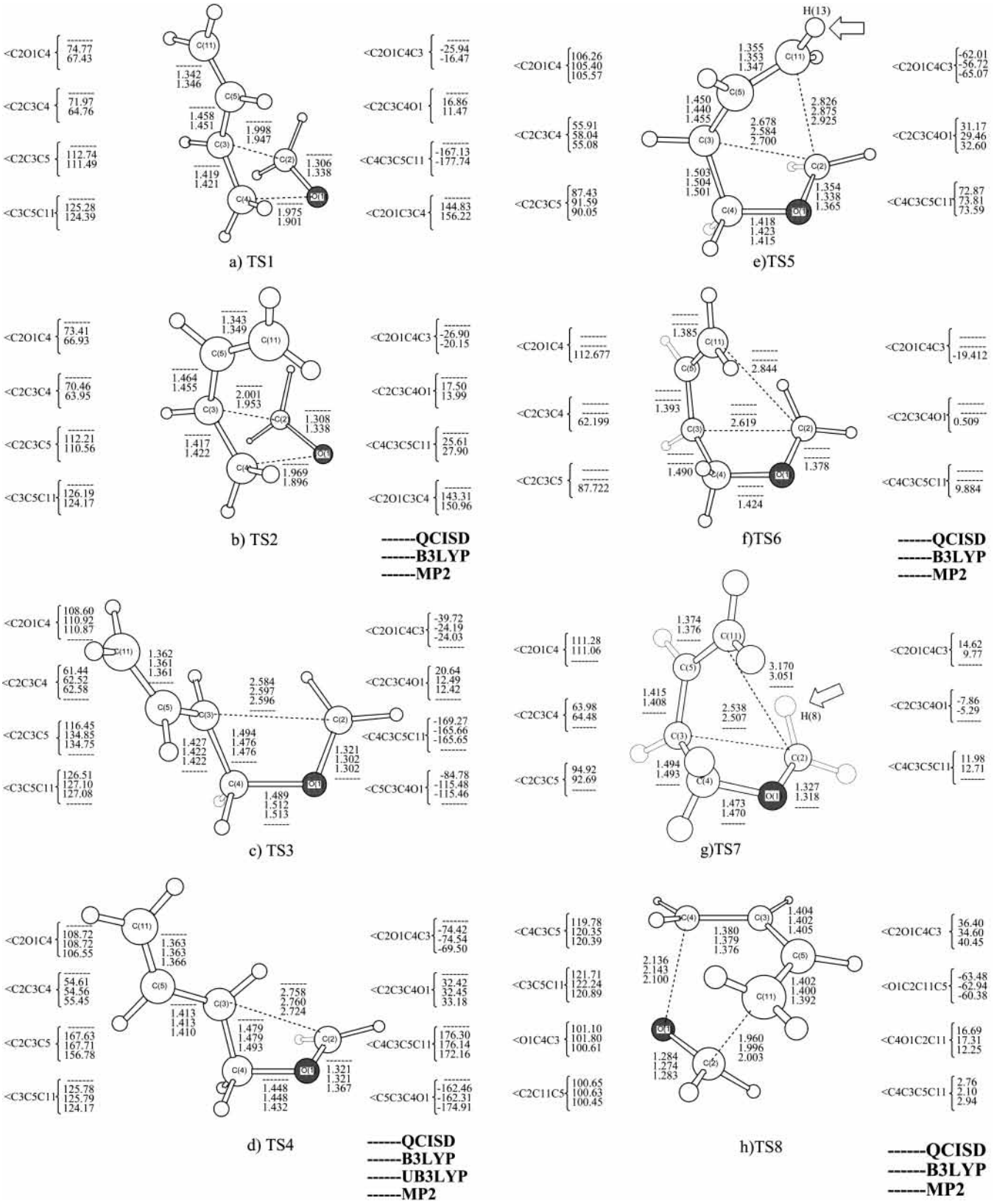

Figure 2. Transition structures located for the processes depicted in Scheme 1. An arrow in both TS5 and TS7 structures pointed toward the respective hydrogen atom assisting the corresponding reaction by a hydrogen type interaction with the π electronic density occurring at the opposite moiety of the supermolecule.

connects the VO1 minimum with the trans products valley and that no other local minimum and no other transition structure were present in the calculated energy profile, which has a slightly flat zone around the TS region. Considering the cycloaddition direction of the reaction, the mechanism through TS3 corresponds to a gauche O(formaldehyde)---C(butadiene, terminal) attack with a "perpendicular" approximation of the reactant causing the pyramidalization of the terminal methylene at C4. A practically constant C3−C4---O1−C2 dihedral angle of about 24° is observed along the IRC pathway, which enables direct cyclization to the VO1 structure (note that the gauche O---C path reported by Robb et al. required a second "rotational"

TABLE 1: Relative Energies and Other Thermodynamic Properties, Computed for All the Stationary Points Located on the Different Scanned PES

	B3LYP/6-31G(d) // B3LYP/6-31G(d)			B3LYP/6-311+G(d,p)// B3LYP/6-31G(d)		
	Eel.+ZPVE(a.u.)	ΔE (kcal/mol)	ΔG (kcal/mol)	Eel.+ZPVE(a.u.)	ΔE (kcal/mol)	ΔG (kcal/mol)
TS1	−270.283539	59.680	59.415	−270.370586	56.035	55.771
TS2	−270.281869	60.727	60.532	−270.368464	57.367	57.172
TS3	−270.285600	58.386	58.185	−270.373076	54.473	54.272
TS4	−270.284534	59.055	59.361	−270.372626	54.755	55.060
TS5	−270.269956	68.203	68.853	−270.354813	65.933	66.584
TS6						
TS7	−270.293365	53.513	54.164	−270.380287	49.948	50.600
TS8	−270.340980	23.635	24.179	−270.425962	21.286	21.830
VO1	−270.378644	0.000	0.000	−270.459884	0.000	0.000
VO2	−270.376355	1.436	1.452	−270.457562	1.457	1.473
DHP	−270.413543	−21.899	−20.829	−270.493041	−20.806	−19.736
tB+for	−270.380312	−1.047	−11.901	−270.470162	−6.450	−17.303
cB+for	−270.374804	2.410	−8.606	−270.464684	−3.012	−14.028
	MP2/6-31G(d)//MP2/6-31G(d)			MP4(SDTQ)/6-311+G(d,p)// MP2/6-31G(d)		
	Eel.+ZPVE(a.u.)	ΔE (kcal/mol)	ΔG (kcal/mol)	Eel.+ZPVE(a.u.)	ΔE (kcal/mol)	ΔG (kcal/mol)
TS1	−269.374470	66.034	65.753	−269.649390	61.236	60.956
TS2	−269.375029	65.683	65.842	−269.648641	61.706	61.865
TS3						
TS4	−269.385178	59.314	59.427	−269.668228	49.415	49.528
TS5	−269.369328	69.260	69.669	−269.649090	61.420	61.834
TS6	−269.383854	60.145	60.795	−269.663480	52.395	53.044
TS7						
TS8	−269.438226	26.026	26.456	−269.694730	32.785	33.215
VO1	−269.479701	0.000	0.000	−269.746976	0.000	0.000
VO2	−269.477806	1.190	1.257	−269.745204	1.112	1.180
DHP	−269.515670	−22.571	−21.625	−269.780179	−20.835	−19.890
tB+for	−269.476756	1.848	−9.229	−269.748720	−1.094	−12.172
cB+for	−269.472464	4.541	−6.579	−269.744554	1.520	−9.601

	QCISD (T)-FC/cc-pVDZ // QCISD-FC/6-31G(d)		
	Eel.+ZPVE (a.u.)	ΔE (kcal/mol)	ΔG (kcal/mol)
TS3	−269.555506	53.500	52.998
TS5	−269.543286	61.168	61.534
TS6			
TS7	−269.557762	52.085	52.234
TS8	−269.596956	27.490	27.791
VO1	−269.640764	0.000	0.000
VO2	−269.638721	1.282	1.332
DHP	−269.675620	−21.873	−21.074
tB+for	−269.645406	−2.913	−14.068
cB+for	−269.640812	−0.030	−11.259

[a] ZPVE computed at the B3LYP/6-31G(d) level. [b] Thermal corrections to the Gibbs energy, computed at the B3LYP/6-31G(d) level (P = 1bar, T = 298.15 K).

transition structure for the cyclization of the intermediate[2]). The addition process through TS3 was suprafacial with respect to both reactants (i.e., a [2_s+2_s] cycloaddition). At MP2/6-31G-(d) the TS3 structure was not found.

Disagreements between DFT and CASSCF predictions on the proper nature of the gauche asynchronous mechanism (one or two kinetic elementary steps, respectively) should arise from the dynamical electronic correlation, which was not included by Robb et al.[2] CASSMP2/6-31G(d)//CASSCF/6-31G(d) single point calculations on Robb's structures computed by us revealed that the gauche biradical intermediate was not stable when dynamical correlation effects are considered at this level.

The most important contributions to the TS4 transition vector are the strongly coupled torsions around the C3−C4 and the O1−C4 bonds. The terminal attacked methylene of butadiene undergoes both a pyramidalization and an internal rotation that amounts about 90° from the original planarity of the butadiene fragment. This rotated methylene suggests that this structure should correlate diabatically with excited states of reactive and/or products. In fact, the IRC calculations from TS4 did not connect with the expected stable minima, but with two high-energy opened structures that were not stable under subsequent optimization on the ground-state PES. Therefore, TS4 is discarded as a transition state for the direct fragmentation of 3-vinyloxetane and would necessitate further investigation.

(c) Stepwise Mechanism through DHP: Ring Expansion Reaction Pathway. The expansion of the oxetane ring to form the six-membered DHP is an intramolecular [1,3]-sigmatropic shift of the methylene group of formaldehyde (at the C2 atom) from C3 to C11 (see Figure 2e,f). For this process to occur, two transitions structures, TS5 (located at all the theoretical models used) and TS6 (only located at the MP2 level), were found (see Figure 2e,f and Scheme 2). The TS5 and TS6 structures correspond to the two Woodward−Hoffmann allowed stereochemical modes of this [1,3]-sigmatropic shift. TS5 (Figure 2e) connects the VO4 minimum (Figure 1b) with the equilibrium structure of 3,6-dihydro-2*H*-pyran (DHP, Figure 1e) by an antarafacial attack without change of configuration at the C2 atom; the so-called $a-r$ path. On the contrary, TS6 (Figure 2f) connects VO2 with DHP and corresponds to a suprafacial

SCHEME 2: Characterized Reaction Channels[a]

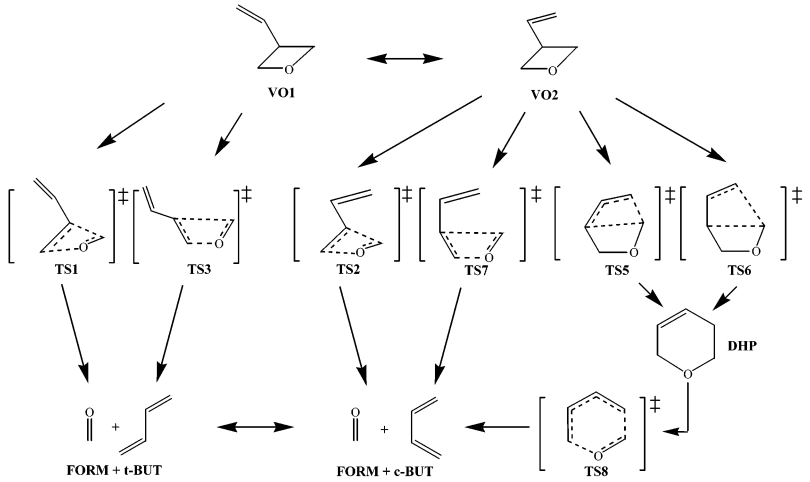

[a] The notation for the stationary points was derived from their order of appearance in the manuscript.

reaction course (relative to the pi conjugated system of the vinyl moiety) with inversion of configuration of the migrating atom C2, i.e., the Woodward−Hoffmann *s*−*i* route. The analysis of transient geometries of the respective IRC pathways has shown that along the *a*−*r* reaction coordinate the supermolecule adopts successive semiboat type conformations but, for the *s*−*i* reaction pathway, the geometry of successive points resembles the equilibrium structure of DHP, i.e., a "quasi" semichair conformation.

Surprisingly, a TS6 type structure was not found on either the RB3LYP or the UB3LYP hypersurfaces. For these theoretical models, saddle-searching routines converged to the TS7 point (Figure 2g and Scheme 2). Although very similar to TS6, IRC paths from this structure revealed that TS7 directly connects the VO2 conformer of 3-vinyloxetane with the formaldehyde + *cis*-butadiene valley, avoiding the formation of DHP along the reaction coordinate. TS7 is the lowest energy transition structure connecting those minima, and so the true transition state for the fragmentation of 3-vinyloxetane, at the B3LYP/6-31G(d) level. At this level, only one transition structure was located for the sigmatropic expansion path, which corresponds to the above-mentioned *a*−*r* route (TS5).

Owing to disagreements between the DFT and the MP*n* results, we carried out QCISD/6-31G(d) geometrical optimizations and subsequent high-level energy refinements (at the QCISD(T)/cc-pVDZ//QCISD/6-31G(d) level) to check the reliability of our DFT and MP*n* predictions. QCISD computed structures (included in Figures 1 and 2) were very similar to those computed by the DFT method (in fact, the QCISD(T)/cc-pVDZ//B3LYP/6-31G(d) theoretical model is becoming a good alternative to study reactivity processes because this represents a combination of high-level energy corrections with less expensive geometry optimizations. In our case, optimizations at the QCISD level were necessary owing to the differences between MP2 and B3LYP computed structures).

Our QCISD calculations also revealed that some structures, like the TS7 one, are extremely sensitive to the basis set quality (the structure computed for TS7 at the QCISD/6-31G level, including no polarization functions, was very close to the MP2 structure computed for TS6).

From the energetic point of view, our best QCISD results (QCISD(T)/cc-pVDZ//QCISD/6-31G(d)) predict, like the DFT calculations, the direct fragmentation, via TS7, as the most favorable reaction channel for the 3-vinyloxetane thermolysis, this conclusion being consistent with the experimentally results by Charless et al.[1a]

Finally, another saddle point, TS8 (Figure 2h and Scheme 2), was located and asigned to the IIb step of Scheme 1 by IRC calculations. The TS8 transition vector describes the concerted cycloreversion process to originate *cis*-butadiene and formaldehyde, or conversely the concerted thermal [4_s+2_s] cycloaddition of butadiene and formaldehyde with "parallel" approximation of the interacting fragments.

(d) Comparison of the Energy Profiles. Figure 3 summarizes the possible competitive reactions for the pyrolysis of 3-vinyloxetane. It was drawn from our best estimated DFT energies. In agreement with experimentally verified facts,[1] our DFT results pointed out that the ring expansion mechanism must be discarded as the origin of the 3-vinyl kinetic effect. On the contrary, MP*n* calculations should lead to wrong conclusions in this respect. (In fact, the asynchronous paths for the vinyloxetane cleavage, or formation, are absent at the MP*n* level.)

TS7 and the TS3 points are transition states for two asynchronous paths that differ from each other in the relative orientation of the vinyl group in the supermolecule (cis in TS7, trans in TS3), in a manner similar to that with TS1 and TS2, for the highly synchronous path. However, the TS3/TS7 pair specially favored the cis rotamer, by 4.5 kcal/mol, contrary to that obtained for the TS1/TS2 pair, with the trans rotamer slightly stabilized (1.4 kcal/mol). This extra stabilization of TS7 appears to be the key for a correct explanation of the studied kinetic effect in the thermolysis of 3-vinyloxetane and will be analyzed in depth in the last section of this work.

The best-estimated DFT activation energy barrier amounts ca. 50 kcal/mol (52 kcal/mol from the best QCISD results). The only experimental data available to confront these values correspond to the 2,4-dimethyl derivative (47.9 ± 1.8 kcal/mol, for the *cis*-2,4-dimethyl-*trans*-3-vinyloxetane[1a]). Thus, our theoretical results compare relatively well, given that the presence of an alkyl group at the C2 position also contributes to the lowering of the activation energy barrier for the oxetane fragmentation, by ca. 4.0 kcal/mol.[1a]

(e) Configurational Analysis of the TSs Wave Functions. To improve the characterization of the electronic rearrangements undergone by the bimolecular transition structures, a two-fragment analysis for the TS1, TS2, TS3, TS7, and TS8 was carried out.[5] Table 2 collects the relative weights (from the c_o

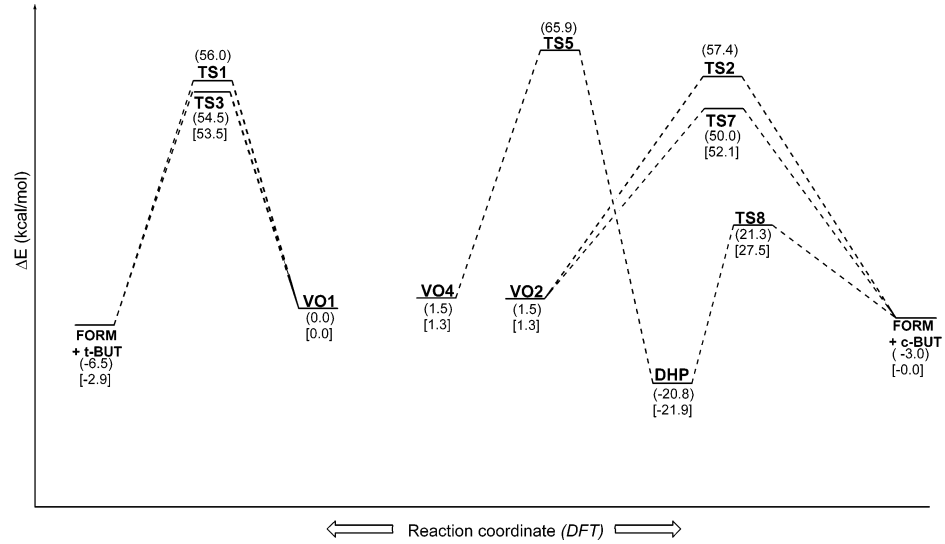

Figure 3. Energy profiles drawn from our best DFT results. In brackets the best QCISD values. Energies including the ZPVE corrections, computed at the B3LYP/6-31G(d) level.

TABLE 2: Relative Weights of the Most Important Fragment Electronic Configurations from Wavefunctions Obtained at the UB3LYP/6-31G(d)//UB3LYP/6-31G(d) Theoretical Level for the Transition States of Cycloreversion Processes (A = H_2CO; B = C_4H_6)

configurations	TS1	TS2	TS3	TS7	TS8
AB	1.0000	1.0000	1.0000	1.0000	1.0000
A^-B^+	0.5468	0.5414	1.1886	1.5695	0.3562
A^+B^-	0.3019	0.3063	0.6193	0.8477	0.1208
$A^{-2}B^{2+}$	0.0982	0.0965	0.6768	0.6251	0.0313
$A^{+2}B^{2-}$	0.0198	0.0205	0.0753	0.1514	0.0033
AB*/A*B	0.1879/0.2187	0.1931/0.2067	0.5589/0.3948	1.0758/0.6333	0.0035/0.0430
AB^{2}*/A^{2}*B	0.0079/0.0279	0.0083/0.0284	0.0673/0.1113	0.2655/0.1071	0.0004/ 0.0001
A^-B^+*/A^-*B^+	0.0072/ 0.0597	0.0064/0.0561	0.0062/0.2425	0.8249/0.5181	0.0018/0.0006
A^+B^-*/A^+*B^-	0.0207/0.0025	0.0221/0.0026	0.1500/0.0081	0.4260/0.1544	0.0019/0.0000
net charge transfer	0.18e	0.18e	0.04e	0.06e	0.18e
Mayer interfrag. order	1.306	1.330	1.655	1.760	1.042

and c_q coefficients in eq 1) of the most important fragment electronic contributions at the UB3LYP/6-31G(d) theoretical level, the computed net charge transfer toward the formaldehyde molecule and the calculated Mayer's interfragment bond orders.[22] As shown in Table 2, there are remarkable differences between the weights of the contributions to the wave function for the synchronous TSs and the asynchronous ones.

For the synchronous TSs (TS1, TS2, or TS8), their wave functions are clearly dominated by the zero AB configuration (A = formaldehyde, B = butadiene) revealing thus their *product-like* character from the point of view of the fragmentation process. The most important electronic interaction between fragments corresponds to the charge transfer from butadiene to formaldehyde (∼0.18 e), mainly through a HOMO (butadiene) → LUMO (formaldehyde; $\Pi^*_{C=O}$) orbital interaction. However, a certain back-donation of charge via NHOMO (formaldehyde; $\Pi_{C=O}$) → LUMO (butadiene) takes place at the TSs. The geometric distortion of the interacting fragments in TS1 and TS2 as evidenced by the C4−C3−C5−C11, C2−O1−C4−C3, and O1−C4−C3−C2 dihedral angles (see Figure 2b) as well as the pyramidalization of the C2 and C4 atoms, favors these electronic interactions and eventually makes possible the symmetry-forbidden $[2_s+2_s]$ cycloaddition. Slight effects of mutual polarization of the fragments (i.e., A*B and AB* configurations) are present in TS1 or TS2 caused by monoexcitations. These effects are of similar amounts in TS1 and TS2 and negligible in TS8, probably due to the greater distance between the fragments in the latter as is reflected in Mayer's interfragment bond orders (see Figure 2h and Table 2).[22] The relevant role of the $\Pi_{C=O}$ (NHOMO) and $\Pi^*_{C=O}$(LUMO) of formaldehyde MO orbitals in the wave function of TS1, TS2, and TS8 would be a direct consequence of a "quasi-parallel" approximation along their respective reaction pathways.

For the asynchronous transition structures, both the TS3 and TS7 wave functions exhibit monotransferred A^-B^+ weights of about 1.19 and 1.57, respectively. Other configurations such as the A^+B^-, $A^{-2}B^{2+}$, single polarized configurations (AB* or A*B), and A^-B^+* (only for TS7), also present large relative weights. Thus, the electronic character of these TSs suggests that the DFT method (UB3LYP/6-31G*) takes into account contributions from excited single states resembling the dominating A^-B^+ configuration (the triplet states would not contribute given that $\langle S^2\rangle = 0$ for all the cases). According to Palmer et al., the asynchronous region for the oxetane formation exhibits avoided crossings because of the closeness of the S_1 and S_0 manifolds.[2] Hence, for the asynchronous paths deeper insight would be gained by high-level multiconfigurational or multireference methodologies (CASPT2, CAS-DFT, etc.).

In the asynchronous structures, the polarization of butadiene dominates over the polarization of formaldehyde. The charge-transfer effects resulted in a more balanced fashion (the net charge transfer toward one of the fragments is small), and the interfragment bond order of Mayer increases. Moreover, for the same configuration, the TS7 weights are generally larger than the TS3 ones, the greatest difference being for the diexcitations: mainly from the monopolarized and monotransferred configuration A^-B^+* (also, in a minor extension, from the A^+*B^-, A^+B^-*, and A^-*B^+configurations). Thus, both the

charge-transfer effects (in the two directions) and the mutual polarization effects contribute to stabilize the TS7 structure.

For the TS3 and TS7 asynchronous structures, the involved MOs are principally the HOMO (butadiene) and the LUMO (formaldehyde; $\Pi^*_{C=O}$). However, the back-donation through the A^+B^- configuration arises now from the nonbonding HOMO (formaldehyde, O lone pair) donating charge to the LUMO (butadiene). These orbital interactions are consistent with a "perpendicular" approximation of the fragments in the TS3 and TS7 structures.

(f) Analysis of the Topology of the Charge Density, $\rho(r)$, and Related Fields. Table 3 collects the obtained values for the charge density, $\rho(r)$, and related quantities, computed at the B3LYP/6-311+G**//B3LYP/6-31G* level, at the BCPs and RCPs for the structures considered in the present study.

In regard to the topology of the charge density $\rho(r)$ of VO1, it is interesting to note that the values of $\rho(r)$, $\nabla^2\rho(r)$ and the eigenvalues λ_1 and λ_2 are very similar for the bonds forming the four-membered ring. Moreover, the like values of λ_1 and λ_2 indicating a preferential accumulation of charge density in perpendicular planes to the bond path involves a low amount of ellipticity. The λ_3 eigenvalue that indicates contraction of charge along the bond path toward the nuclei is lower than λ_1 and λ_2, thus confirming that reasoning. The strongest bond as measured by the local energy density, $H(r) = -K(r)$, is the terminal double bond of the vinyl group, followed by C−O bonds, C−C bonds of the ring are a bit weaker than the adjacent C−C bond. These results are consistent with the geometry of the asynchronous transition states calculated, in which the C−C bond is broken in a major extension compared with the C−O bond (this is also true for the synchronous ones).

The topology of $\rho(r)$ in TS1 and TS2 exhibits one ring critical point for both TSs. The breaking bonds are well characterized by the appearance of the corresponding BCPs on the interaction line between the nuclei. The values of $\rho(r)$ and related quantities increase for the C−O forming bond. Particularly interesting are the ellipticity and the λ_3 eigenvalue for the C−O BCP. Yet this bond does not still present the characteristic values of a C−O typical bond (cf. ref 6). The ellipticity is increased for all the bonds except the terminal bond of the vinyl group, indicating π-density reorganization in the TS. Notably, the ellipticities for the breaking bonds (C4−O1 and C2−C3 in Figure 2b) of TS2 are larger than those for TS1.

In TS3 and TS7 the topology of $\rho(r)$ renders no ring critical point and no BCP between the C3 and the C2 nuclei probably due to the long distance existing between them. In comparing these TSs with the synchronous ones (i.e., TS1 and TS2), one sees that the nature of the C−O bond to be formed is different: they exhibit a low value for $-\nabla^2\rho(r)$, a great λ_3 (1.24 and 1.13, respectively), and also similar values of K_c and G_c. These values are characteristic of the carbonyl bond type: on one side is a strong shared interaction (see $-K_c = -0.49193$ and -0.46574, respectively) having so a large ρ_c (0.30849 and 0.31301, respectively) and at the same time the charge is also "pushed" toward the nuclei (or to the O atom) along the bond path (indicated by large both λ_3 and G_c). Therefore, the charge undergoes a tension at the interatomic surface, thus accounting for the polarization usually ascribed to this bond (pictorially: C═O ↔ C^+—O^-). Therefore, the asynchronous TSs are later than the synchronous ones regarding the C−O bond formation.

For the TS7 structure an unexpected "hydrogen-bond" type interaction appears in $\rho(r)$, which is necessary to fulfill the Poincaré−Hopf relationship. The corresponding BCP lies on the interaction line between the H8 atom (attached to C2) and the C11 atom (at the B3LYP/6-31G(d)//B3LYP/6-31G(d) level both an extra RCP and an extra BCP appear that disappear at the B3LYP/6-311+G(d,p)//B3LYP/6-31G(d,p) level). The bond path connecting the involved nuclei was analytically obtained with the EXT94b program.

Equally, another "hydrogen-bond" interaction appears in $\rho(r)$ for the ring-expansion transition structure (TS5). However, this extra BCP is in the interaction line between the H13 atom (attached to C11) and the C2 atom (see Figure 2e). As shown from the values of $\rho(r)$ and $\nabla^2\rho(r)$ at the corresponding BCPs, the TS7 interaction is stronger than the TS5 one (values of 0.02396 and 0.07187, respectively, for TS7, vs 0.01973 and 0.04772 values, for TS5).

Therefore, both the asynchronous direct fragmentation (via TS7) and the ring expansion process to bring out the six-memberred ring (via TS5) are assisted by the respective "H-bond" interactions described above. More insight can be gained by observing the geometrical changes of the two transition structures along their respective IRC paths. In the TS7 path, the hydrogen atom attached to C2(−O) evolves by passing in front of the π system of the vinyl moiety, and hence assisting the direct fragmentation.

On the other hand, the vinyl group rearranges in TS5 to form the H-interaction (compare the C4−C3−C5−C11 dihedral angle values in Figure 2e,f), breaking the vinyl conjugation (ϵ for C4−C5 is only 0.12671 for TS5, against 0.21572 for TS7), accounting for the extra amount of energy needed (see Figure 3).

To further check these assumptions, the vinyl group was substituted by a formyl one. In doing so, one should expect a stronger H-bond, for the analogous TS7, between the H−(CO) and the oxygen of the formyl group. In effect, this was the case and the resultant interaction exhibited a greater amount of $\rho(r)$ and $\nabla^2\rho(r)$ in absolute value (these were evaluated only at the B3LYP/6-31G(d)//B3LYP/6-31G(d) level).

Conclusions

Our study on the kinetic C3-vinyl substitution effect in oxetanes allows us to characterize transition states for all the elementary chemical reactions involved in the thermal fragmentation of these compounds. Concerning the direct fragmentation of oxetane (route I in Scheme 1), our results predicted the possibility of synchronous and asynchronous concerted paths. However, for the asynchronous path no biradical minimum was obtained. The two-step pathway, which implies a ring expansion, has been also studied and must be discarded as the origin of the C3-vinyl kinetic effect in oxetane thermal fragmentation. An asynchronous concerted path, assisted by a hydrogen bond type interaction with the π-system of the vinylic moiety of the supermolecule, gave the most favorable reaction channel and would explain the kinetic effect observed in oxetanes upon symmetric substitution by a vinylic group.

A comparative configurational analysis of transition-state wave functions allowed us to elucidate the more important fragment interactions and the role of frontier and nonfrontier molecular orbitals along the synchronous and asynchronous reaction pathways. Moreover, the analysis of the topology of the $\rho(r)$ in the framework of Bader's atoms in molecules theory revealed the existence of an unexpected H-interaction that assists two of the studied processes and ultimately determines the most favorable reaction path.

Finally, the chemical system studied in this article appears as a good candidate to check the performance of the new theoretical tools (CAS-DFT, GVB-DFT, ...) that are in progress

TABLE 3: Values of the Charge Density $\rho(r)$ and Related Magnitudes[a] Computed at the B3LYP/6-311+G(d,p)//B3LYP/6-31G(d) Level Evaluated at the BCPs and RCPs for the Structures Considered in the Present Study

	ρ_c	$\nabla^2\rho_c$	λ_1	λ_2	λ_3	ϵ	$-K_c$	G_c
				VO1				
C2−O1	0.25142	−0.54113	−0.47433	−0.45706	0.39025	0.03777	−0.31381	0.17853
C4−O1	0.25142	−0.54112	−0.47433	−0.45706	0.39025	0.03777	−0.31381	0.17853
C3−C2	0.23547	−0.50891	−0.44225	−0.43528	0.36863	0.01602	−0.18286	0.05563
C4−C3	0.23548	−0.50892	−0.44226	−0.43529	0.36863	0.01602	−0.18286	0.05563
C5−C3	0.25857	−0.62892	−0.50247	−0.48331	0.35686	0.03964	−0.21856	0.06133
C11−C5	0.34108	−1.00586	−0.74121	−0.55218	0.28753	0.34235	−0.38750	0.13604
RCP	0.09024	0.42891	−0.13310	0.25944	0.30257			
				TS1				
C2−O1	0.34528	−0.76877	−0.83433	−0.74071	0.80627	0.12639	−0.53113	0.33894
C4−O1	0.06881	0.16970	−0.8126	−0.03541	0.28636	1.29498	−0.00932	0.05174
C3−C2	0.08775	0.03394	−0.11366	−0.06637	0.21398	0.71246	−0.02891	0.03739
C4−C3	0.29457	−0.78515	−0.60194	−0.50345	0.32025	0.19563	−0.29458	0.09829
C5−C3	0.27271	−0.68852	−0.54855	−0.48644	0.34647	0.12768	−0.24481	0.07268
C11−C5	0.33535	−0.97566	−0.72426	−0.54320	0.29179	0.33333	−0.37531	0.13140
RCP	0.06679	0.17533	−0.08284	0.03068	0.22749			
				TS2				
C2−O1	0.34379	−0.77557	−0.82609	−0.73500	0.78552	0.12393	−0.52715	0.33326
C4−O1	0.07018	0.17473	−0.08398	−0.02132	0.28003	2.93876	−0.00952	0.05320
C3−C2	0.08808	0.04097	−0.11687	−0.05360	0.21144	1.18056	−0.02821	0.03846
C4−C3	0.29543	−0.78862	−0.60399	−0.50440	0.31928	0.19645	−0.29706	0.09991
C5−C3	0.26979	−0.67320	−0.54097	−0.47911	0.34688	0.12913	−0.23959	0.07129
C11−C5	0.33413	−0.96703	−0.71893	−0.54038	0.29228	0.33042	−0.37298	0.13122
RCP	0.06975	0.17621	−0.08656	0.01970	0.24308			
				TS3				
C2−O1	0.32522	−0.18053	−0.74277	−0.67411	1.23635	0.10185	−0.49193	0.44680
C4−O1	0.20131	−0.27255	−0.32741	−0.30988	0.36473	0.05657	−0.21422	0.14608
C3−C2								
C4−C3	0.26621	−0.65047	−0.51995	-0.47699	0.34647	0.09005	−0.23530	0.07269
C5−C3	0.29009	−0.76093	−0.59660	-0.50079	0.33647	0.19130	−0.27831	0.08808
C11−C5	0.32414	−0.92326	−0.69171	-0.53594	0.30439	0.29064	−0.35014	0.11932
RCP								
				TS5				
C2−O1	0.30203	−0.27872	−0.62985	−0.59617	0.94730	0.05650	−0.44251	0.37283
C4−O1	0.24955	−0.36515	−0.45288	−0.42560	0.51333	0.06410	−0.32998	0.23870
C4−C3	0.25431	-0.59180	−0.50275	−0.45483	0.36577	0.10535	−0.21154	0.06359
C5−C3	0.28053	−0.71637	−0.50678	−0.49771	−0.34212	0.12671	−0.26004	0.08095
C11−C5	0.33005	-0.95788	−0.71248	-0.54852	0.30312	0.29891	−0.36190	0.12243
H13−C2	0.01973	0.04772	−0.01638	-0.01297	0.07707	0.26289	+0.00122	0.01071
RCP	0.01482	0.05462	−0.00810	0.01754	0.04518			
				TS7				
C2−O1	0.31301	−0.20413	−0.68822	−0.64620	1.13028	0.06503	−0.46574	0.41470
C4−O1	0.22183	−0.31530	−0.36568	−0.34520	0.39558	0.05931	−0.26817	0.18934
C4−C3	0.26056	−0.63099	−0.50716	−0.47870	0.35488	0.05944	−0.22333	0.06558
C5−C3	0.298801	−0.79829	−0.62007	−0.51004	0.33181	0.21572	−0.29504	0.09547q
C11−C5	0.31514	−0.87336	−0.66263	−0.52289	0.31216	0.26724	−0.33072	0.11238
H8−C11	0.02396	0.07187	−0.02585	−0.01114	0.10886	1.32025	+0.00212	0.01585
RCP	0.02180	0.09503	−0.02251	0.00969	0.10785			
				TS8				
C2−O1	0.35455	−0.34309	−0.81947	−0.79994	1.27632	0.02441	−0.55948	0.47371
C4−O1	0.04985	0.12229	−0.06081	−0.04393	0.22703	0.38417	−0.00192	0.03250
C11−C2	0.08350	0.01250	−0.10799	−0.09634	0.21683	0.12092	−0.02664	0.02977
C4−C3	0.31715	−0.90358	−0.66804	-0.55189	0.31634	0.21046	−0.33391	0.10801
C5−C3	0.30311	−0.83369	−0.63269	−0.53118	0.33018	0.19109	−0.30447	0.09605
C11−C5	0.30464	−0.83649	−0.63137	−0.53366	0.32854	0.18310	−0.30725	0.09813
RCP	0.01432	0.08286	−0.00772	0.03528	0.05530			
				DHP				
C2−O1	0.25470	−0.47206	−0.46660	−0.45994	0.45447	0.01448	−0.33069	0.21268
C4−O1	0.25784	−0.49884	−0.48314	−0.47043	0.45472	0.02702	−0.33632	0.21161
C11−C5	0.25075	−0.59172	−0.48030	−0.46361	0.35219	0.03600	−0.20742	0.05949
C11−C2	0.24599	−0.56714	−0.47529	−0.46050	0.36864	0.03212	−0.3212	0.19698
C4−C3	0.25636	−0.62153	−0.50950	−0.47598	0.36395	0.07043	−0.21428	0.05889
C5−C3	0.34034	−0.98869	−0.73654	−0.54042	0.28827	0.36292	−0.38590	0.13873
RCP	0.02055	0.13881	−0.01373	0.06849	0.08405			

[a] ρ_c, $\nabla^2\rho_c$, E_c, and G_c stand for the amount of charge density, laplacian, electronic energy density (that equals the minus kinetic energy density, $-K_c$), and kinetic energy density, respectively, evaluated at the corresponding bond critical point. λ_1, λ_2, and λ_3 are the eigenvalues of the Hessian matrix of $\rho(\mathbf{r})$ evaluated at the BCP, and ϵ is the ellipticity defined as $\epsilon = \lambda_1/\lambda_2 - 1$. All quantities are in atomic units.

within the DFT methodology to improve the treatment of multireference problems, particularly if multideterminantal formulations are required and/or if strong static correlation effects are present.[10c]

Acknowledgment. We thank Prof. Dimas Suárez (at Oviedo University) for the cession of the ANACAL software and valuable suggestions on the manuscript preparation. Also, to CIEMAT (Madrid) and SCAI (University of Málaga) for the generous allocation of computer time.

References and Notes

(1) (a) Carless, H. A. J.; Maitra, K. *J. Chem. Soc., Faraday Trans. I* **1980**, *76*, 1849 and references therein. (b) Imai, T.; Nishida, S. *Chem. Lett.* **1980**, 41. (c) Zalotai, L.; Bérces T.; Márta, F. *J. Chem. Soc., Faraday Trans.* **1990**, *86*, 21. (d) Holbrook, K. A.; Scott, R. A. *J. Chem. Soc., Faraday Trans. I* **1974**, *70*, *43*. (e) Jones, G., II.; Staires, J. C. *Tetrahedron Lett.* **1974**, *24*, 2099.

(2) Palmer, I. J.; Ragazos, I. N.; Bernardi, F.; Olivucci M.; Robb, M. A. *J. Am. Chem. Soc*. **1994**, *116*, 2121.

(3) Bordejé, M. C.; Mo, O.; Yañez, M.; Herreros, M.; Abboud, J. L. M. *J. Am. Chem. Soc.* **1993**, *115*, 7389.

(4) Parr, R. G.; Yang, W. In *Density Functional Theory of Atoms and Molecules*; Oxford University Press: New York, 1989.

(5) (a) Menéndez, M. I.; Sordo, J. A.; Sordo, T. L. *J. Phys. Chem.* **1992**, *96*, 1185. (b) López, R.; Menéndez, M. I.; Suárez D.; Sordo, T. L.; Sordo, J. A. *Comput. Phys. Commun.* **1993**, *76*, 235. (c) For example: Menéndez, M. I.; González, J.; Sordo, J. A.; Sordo, T. L. *J. Mol. Struct. (THEOCHEM)* **1994**, *309*, 295 and references therein. (d) Suárez D.; Sordo, T. L.; Sordo, J. A. *J. Org. Chem.* **1995**, *60*, 2848.

(6) (a) Bader, R. W. F. In *Atoms In Molecules. A quantum theory*; Oxford University Press: New York, 1990. (b) Popelier, P. L. A. In *Atoms In Molecules: An Introduction*; Pearson Education: Harlow, U.K., 2000.

(7) Frisch, M. J.; Trucks, G. W.; Schlegel, H. B.; Scuseria, G. E.; Robb, M. A.; Cheeseman, J. R.; Zakrzewski, V. G.; Montgomery, J. A., Jr.; Stratmann, R. E.; Burant, J. C.; Dapprich, S.; Millam, J. M.; Daniels, A. D.; Kudin, K. N.; Strain, M. C.; Farkas, O.; Tomasi, J.; Barone, V.; Cossi, M.; Cammi, R.; Mennucci, B.; Pomelli, C.; Adamo, C.; Clifford, S.; Ochterski, J.; Petersson, G. A.; Ayala, P. Y.; Cui, Q.; Morokuma, K.; Malick, D. K.; Rabuck, A. D.; Raghavachari, K.; Foresman, J. B.; Cioslowski, J.; Ortiz, J. V.; Stefanov, B. B.; Liu, G.; Liashenko, A.; Piskorz, P.; Komaromi, I.; Gomperts, R.; Martin, R. L.; Fox, D. J.; Keith, T.; Al-Laham, M. A.; Peng, C. Y.; Nanayakkara, A.; Gonzalez, C.; Challacombe, M.; Gill, P. M. W.; Johnson, B. G.; Chen, W.; Wong, M. W.; Andres, J. L.; Head-Gordon, M.; Replogle, E. S.; Pople, J. A. *Gaussian 98*; Gaussian, Inc.: Pittsburgh, PA, 1998.

(8) (a) Becke, A. D. *J. Phys. Chem.* **1993**, *98*, 5648. (b) Becke, A. D. *Phys. Rev. B* **1988**, *38*, 3098. (c) Lee, C.; Yang, W.; Parr, R. G. *Phys. Rev. B* **1988**, *37*, 785.

(9) Hehre, W. J.; Radom, L.; Pople, J. A.; Schleyer, P. v. R. In *Ab Initio Molecular Orbital Theory*; John Wiley & Sons: New York, 1986.

(10) (a) Cremer, D.; Kraka, E.; Szalay, P. G. *Chem. Phys. Lett*. **1998**, *292*, 97. (b) He, Y.; Gräfenstein, J.; Kraka, E.; Cremer, D. *Mol. Phys.* **2000**, *98*, 1639. (c) Gräfenstein, J.; Cremer, D. *Phys. Chem. Chem. Phys.* **2000**, *2*, 2091. (d) Gräfenstein, J.; Hjerpe, A.; Kraka, E.; Cremer, D. *J. Phys. Chem. A* **2000**, *104*, 1748 (e) Houk, K. N.; Beno, B. R.; Nendel, M.; Black, K.; Yoo, H. Y.; Eilsey, S.; Lee, J. K. *J. Mol. Struct. (THEOCHEM)* **1997**, 398−399, 169. (f) Goldstein, E.; Beno, B. R.; Houk, K. N. *J. Am. Chem. Soc.* **1996**, *118*, 6036. (g) Wiest, O.; Montiel, D. C.; Houk, K. N. *J. Phys. Chem. A* **1997**, *101*, 8378.

(11) Jarzecki, A. A.; Gajewski, J.; Davidson, E. R. *J. Am. Chem. Soc.* **1999**, *121*, 6928.

(12) Schlegel, H. B. *J. Comput. Chem*. **1982**, *3*, 211.

(13) Møller, C.; Plesset, M. S. *Phys. Rev.* **1934**, *46*, 618.

(14) Pople, J. A.; Head-Gordon, M.; Raghavachari, K. *J. Chem. Phys.* **1987**, *87*, 5968.

(15) Dunning, T. H. Jr. *J. Chem. Phys.* **1989**, *90*, 1007.

(16) See, for example: (a) Staroverov, V. N.; Davidson, E. R. *J. Mol. Struct. (THEOCHEM)* **2001**, *573*, 81. (b) Davidson, E. R. *Chem. Phys. Lett.* **2001**, *284*, 301. (c) Parkinson, C. J.; Mayer, P. M.; Radom, L. *Theor. Chem. Acc.* **1999**, *102*, 92.

(17) Fukui, K. *Acc. Chem. Res.* **1981**, *14*, 363.

(18) González, C.; Schlegel, H. B. *J. Phys. Chem.* **1990**, *94*, 5523.

(19) Fujimoto, H.; Kato, S.; Yamabe, S.; Fukui, K. *J. Chem. Phys.* **1972**, *60*, 572.

(20) (a) AIMPAC suite is developed at McMaster University by R. V. F. Bader and co. (b) MORPHY1.0; Popelier, P. L. A., *Comput. Phys. Comm.* **1996**, *93*, 212. (c) MORPHY 98, a program written by P. L. A. Popelier with a contribution from R. G. A. Bone, UMIST, Manchester, England, EU 1998.

(21) Bernardi, F.; Bottoni, A.; Olivucci, M.; Venturini, A.; Robb, M. A. *J. Chem. Soc., Faraday Trans.* **1994**, *90*, 1617.

(22) Mayer, I. *Int. J. Quantum Chem.* **1986**, *29*, 73 and 477.